INSTITUT DE FRANCE
Académie des sciences

Comptes Rendus

Physique

Benedikt Weger, Satyapriya Gupta and Thomas Hochrainer

Analysing discrete dislocation data using alignment and curvature tensors

Volume 22, issue S3 (2021), p. 249-266

<https://doi.org/10.5802/crphys.60>

Part of the Special Issue: Plasticity and Solid State Physics

Guest editors: Samuel Forest (Mines ParisTech, Université PSL, CNRS, France) and David Rodney (Université Claude Bernard Lyon 1, France)

Comptes Rendus
Physique
2021, 22, nº S3, p. 249-266
https://doi.org/10.5802/crphys.60

Plasticity and Solid State Physics / *Plasticité et Physique des Solides*

Analysing discrete dislocation data using alignment and curvature tensors

Benedikt Weger [a], **Satyapriya Gupta** [a] **and Thomas Hochrainer** [*, a]

[a] Institut für Festigkeitslehre, Technische Universität Graz, Kopernikusgasse 24, 8010 Graz, Austria

E-mails: benedikt.weger@tugraz.at (B. Weger), satyapriya.gupta@tugraz.at (S. Gupta), hochrainer@tugraz.at (T. Hochrainer)

Abstract. Analysis of large scale discrete dislocation data requires the characterisation of complex dislocation networks by suitable average quantities. In the current work, we suggest dislocation alignment tensors and closely related curvature tensors as easily extractable and intelligible measures of geometrical and topological characteristics of dislocation distributions. We provide formulae for extracting these measures from discrete dislocation data based on straight segments. Examples for interpreting and visualising these measures are provided for a simple configuration and two more involved results from discrete dislocation simulations. We suggest the alignment and curvature tensors for wider use in plasticity research.

Keywords. Discrete dislocation simulations, Dislocation alignment tensors, Dislocation curvature tensors, Data analysis, Plasticity, Microstructure.

Available online 3rd May 2021

1. Introduction

Recent years have seen the establishment of large scale data analysis tools in computational materials science, see, e.g., [1] for a recent review. Dislocation based crystal plasticity is still one of the least understood areas of materials research. Thanks to recent progress in discrete dislocation (DD) simulations and extremely large scale molecular dynamics simulations, there are now large data sets on dislocation distributions available for analysis (e.g. [2, 3]). However, it seems that there is a shortage of meaningful measures for quantifying the content of complex dislocation networks. Classical measures are Kröner's dislocation density tensor [4] and the total dislocation density, where the latter is usually classified by slip system or Burgers vector. However, the Kröner tensor, as a measure of geometrically necessary dislocations, is well know to be strongly scale dependent—typically representing only a small fraction of the total dislocation content if evaluated for volumes containing a considerable number of dislocations, e.g. [5]. On the other hand, the total dislocation density does not carry any orientation information and is thus ignorant to dominant dislocation characters which may develop upon deformation.

* Corresponding author.

Moreover, the total dislocation density does not comprise any topological information and may, for example, not distinguish a small number of large dislocation loops from a high number of small loops; but these two cases represent very different dynamics in further deformation. Besides these classical measures, the link length distribution has been considered recently [6, 7], which comprises interesting characteristics of dislocation networks. However, what appears to be mostly overlooked is that there exist more refined dislocation density measures developed in the community dealing with so-called continuum dislocation dynamics (CDD); and that these measures are easy to obtain and relevant for characterising discrete dislocation states. These so-called dislocation alignment tensors [8] allow for a seamless characterisation of orientation distributions of dislocation lines. Some of these CDD variables have been obtained from DD simulations in [9] and [10], where in the latter the second order alignment tensor has been found to be of significance in a specific machine learning task. However, these two studies employed a special DD code based on parametrised dislocations and a method termed discrete-to-continuum framework (D2C). This possibly gave the impression that obtaining the CDD variables would rely on smooth curves and their conversion into smooth fields. In addition, these works do not put much effort in explaining the content and interpretation of the alignment tensors or curvature variables. Therefore, the current paper is supposed to fill two gaps in the literature: (i) to demonstrate how easily these measures may be obtained from more conventional DD codes based on dislocation line segments (Section 2) and (ii) to provide interpretations of the content of these measures for simple and reasonably complex dislocation configurations (Section 3). Moreover, we summarise the results and briefly suggest dislocation alignment tensors for further use in plasticity research in Section 4.

2. Obtaining alignment tensors from discrete dislocation data

Alignment tensors are well-established in other areas dealing with "random" distributions of directed or line-like objects, for example, in the realms of liquid crystals, polymers, fibre-reinforcements, and soft-matter physics (e.g. [11–13]). The term "alignment tensor" stems mostly from the symmetric second order alignment tensor, where the alignment of fibres displays in the (non-negative) eigenvalues—where a spherical tensor with three equal eigenvalues represents an isotropic, maximally non-aligned distribution, while a single non-zero eigenvalue indicates complete alignment of fibres in the associated eigendirection. In many areas, solely the second order alignment tensor is considered, which usually results from the fact that the directed objects are not oriented, in that there is no distinguished line-sense for continuous curves or a head-tail symmetry for short objects. This makes all odd-degree alignment tensors vanish. This is different in case of dislocations, because, upon choosing the sign of the Burgers vector, dislocation lines are oriented curves. The first order alignment tensor (a vector), for instance, is closely related to the classical dislocation density tensor. Another peculiarity of dislocation systems is that they evolve over time. In the evolution of the alignment tensors, there appear average measures of dislocation curvature, which determine dislocation multiplication. Therefore, a complete set of CDD variables also contains measures of dislocation curvature, which are intricately related to the alignment tensors and, in special cases, may be interpreted as a sort of "number density" of dislocations. In the realm of dislocations, alignment tensors have been introduced as an expansion of a higher dimensional theory based on quantities distributed in orientation space [8]. We shall not resort to this origin, but rather introduce the alignment tensors based on dislocation curves and their segments. We begin with assuming smooth curves, although we note that due to dislocation reactions or cross slip, dislocations will usually not be smooth but involve corners.

For the time being, let the dislocation lines be smooth curves $c_m^{\boldsymbol{b}}$ classified by Burgers vector $\boldsymbol{b}$, where $m \in \{1,\dots,M(\boldsymbol{b})\}$ and $M(\boldsymbol{b})$ denotes the number of dislocations with Burgers vector

$\boldsymbol{b}$. Besides elementary Burgers vectors, this could also comprise compound Burgers vectors of dislocation junctions. The treatment of junctions is unproblematic for the dislocation alignment tensors, however, it requires special care for the curvature variables which we will not detail in the current contribution.

We regard a fixed volume V and denote with $c^{\boldsymbol{b}}_{m,V} := V \cap c^{\boldsymbol{b}}_m$ the curve segment resulting from intersection with V.[1] The curve segments $c^{\boldsymbol{b}}_{m,V}$ are supposed to be parametrised by a parameter $s \in [0, S^{\boldsymbol{b}}_{m,V})$, which is chosen to be consistent with the line sense resulting from choosing the sign of the Burgers vector. Let furthermore

$$\partial_s \boldsymbol{c}^{\boldsymbol{b}}_m(s) := \frac{\mathrm{d}\boldsymbol{c}^{\boldsymbol{b}}_m(s)}{\mathrm{d}s} \tag{1}$$

be the non-normalised tangent vector to the curve, while the normalised tangent direction is

$$\boldsymbol{l}^{\boldsymbol{b}}_m(s) := \frac{\partial_s \boldsymbol{c}^{\boldsymbol{b}}_m(s)}{\left|\partial_s \boldsymbol{c}^{\boldsymbol{b}}_m(s)\right|}. \tag{2}$$

The length of a dislocation segment $L^{\boldsymbol{b}}_{m,V}$ is obtained via integration as

$$L^{\boldsymbol{b}}_{m,V} = \int_0^{S^{\boldsymbol{b}}_{m,V}} \left|\partial_s \boldsymbol{c}^{\boldsymbol{b}}_m(s)\right| \mathrm{d}s. \tag{3}$$

The average scalar or zeroth-order alignment tensor of the volume V is the total dislocation density,

$$\rho = \frac{1}{|V|} \sum_{\boldsymbol{b}} \sum_{m=1}^{M(\boldsymbol{b})} \int_0^{S^{\boldsymbol{b}}_{m,V}} \left|\partial_s \boldsymbol{c}^{\boldsymbol{b}}_m(s)\right| \mathrm{d}s = \frac{1}{|V|} \sum_{\boldsymbol{b}} \sum_{m=1}^{M(\boldsymbol{b})} L^{\boldsymbol{b}}_{m,V}. \tag{4}$$

The average first order alignment tensor is given by the sum over the vectors connecting the points, where the intersecting dislocations enter and leave the volume. We rewrite this as integral of the tangent vector, such that

$$\boldsymbol{\rho}^{(1)} = \frac{1}{|V|} \sum_{\boldsymbol{b}} \sum_{m=1}^{M(\boldsymbol{b})} \left(\boldsymbol{c}^{\boldsymbol{b}}_m(S_{m,V}) - \boldsymbol{c}^{\boldsymbol{b}}_m(0)\right) \tag{5}$$

$$= \frac{1}{|V|} \sum_{\boldsymbol{b}} \sum_{m=1}^{M(\boldsymbol{b})} \int_0^{S^{\boldsymbol{b}}_{m,V}} \partial_s \boldsymbol{c}^{\boldsymbol{b}}_m(s) \mathrm{d}s = \frac{1}{|V|} \sum_{\boldsymbol{b}} \sum_{m=1}^{M(\boldsymbol{b})} \int_0^{S^{\boldsymbol{b}}_{m,V}} \boldsymbol{l}^{\boldsymbol{b}}_m(s) \left|\partial_s \boldsymbol{c}^{\boldsymbol{b}}_m(s)\right| \mathrm{d}s. \tag{6}$$

Most notably for the first order alignment tensor, but in fact for all alignment tensors including the total dislocation density, it makes sense to define the tensors classified by Burgers vector (or, alternatively, by slip system), i.e.,

$$\rho^{\boldsymbol{b}} = \frac{1}{|V|} \sum_{m=1}^{M(\boldsymbol{b})} L^{\boldsymbol{b}}_{m,V} \quad \text{and} \tag{7}$$

$$\boldsymbol{\rho}^{(1),\boldsymbol{b}} = \frac{1}{|V|} \sum_{m=1}^{M(\boldsymbol{b})} \int_0^{S^{\boldsymbol{b}}_{m,V}} \partial_s \boldsymbol{c}^{\boldsymbol{b}}_m(s) \mathrm{d}s = \frac{1}{|V|} \sum_{m=1}^{M(\boldsymbol{b})} \int_0^{S^{\boldsymbol{b}}_{m,V}} \boldsymbol{l}^{\boldsymbol{b}}_m(s) \left|\partial_s \boldsymbol{c}^{\boldsymbol{b}}_m(s)\right| \mathrm{d}s, \tag{8}$$

such that

$$\rho = \sum_{\boldsymbol{b}} \rho^{\boldsymbol{b}} \quad \text{and} \tag{9}$$

$$\boldsymbol{\rho}^{(1)} = \sum_{\boldsymbol{b}} \boldsymbol{\rho}^{(1),\boldsymbol{b}}. \tag{10}$$

[1] For simplicity, we neglect in this notation the possibility that the intersection of a curve with the volume results in several separate segments of the curve. The consideration of this case would solely modify the numbering of the curve segments to be summed over in the following.

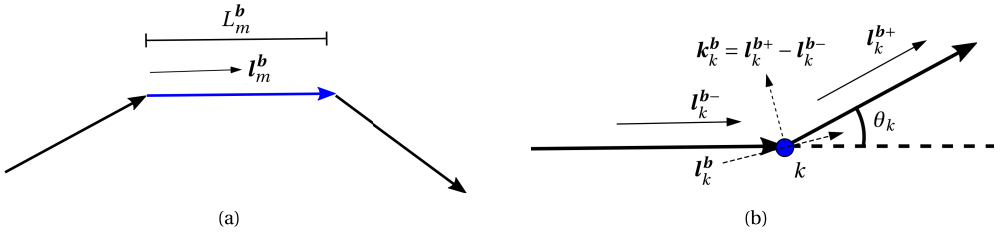

Figure 1. Schematic representation of geometric quantities employed in the segment based calculations, (a) line direction and length of a segment; (b) discrete average tangent and curvature vector at a node for two segments in a common plane.

From the first order alignment tensors classified by Burgers vector, we obtain the average dislocation density tensor $\boldsymbol{\alpha}$ (of geometrically necessary dislocations, GNDs) of the volume V by

$$\boldsymbol{\alpha} = \sum_{\boldsymbol{b}} \boldsymbol{\rho}^{(1),\boldsymbol{b}} \otimes \boldsymbol{b}. \tag{11}$$

The second order alignment tensor classified by Burgers vector is defined as

$$\boldsymbol{\rho}^{(2),\boldsymbol{b}} = \frac{1}{|V|} \sum_{m=1}^{M(\boldsymbol{b})} \int_0^{S_{m,V}^{\boldsymbol{b}}} \boldsymbol{l}_m^{\boldsymbol{b}}(s) \otimes \boldsymbol{l}_m^{\boldsymbol{b}}(s) \left| \partial_s \boldsymbol{c}_m^{\boldsymbol{b}}(s) \right| \mathrm{d}s, \tag{12}$$

and, accordingly, the nth order tensors are expressed as

$$\boldsymbol{\rho}^{(n),\boldsymbol{b}} = \frac{1}{|V|} \sum_{m=1}^{M(\boldsymbol{b})} \int_0^{S_{m,V}^{\boldsymbol{b}}} \underbrace{\boldsymbol{l}_m^{\boldsymbol{b}}(s) \otimes \cdots \otimes \boldsymbol{l}_m^{\boldsymbol{b}}(s)}_{n\text{-times}} \left| \partial_s \boldsymbol{c}_m^{\boldsymbol{b}}(s) \right| \mathrm{d}s. \tag{13}$$

Obviously, the total nth order alignment tensors are defined by summing over the Burgers vectors,

$$\boldsymbol{\rho}^{(n)} = \sum_{\boldsymbol{b}} \boldsymbol{\rho}^{(n),\boldsymbol{b}}. \tag{14}$$

We note that the integral definitions employed for the alignment tensors also work for piecewise differentiable curves, particularly for polygonal descriptions based on straight segments, as frequently employed in discrete dislocation simulations. When the considered curve segments are straight, the line-direction is a constant vector, independent of the parameter s, $\boldsymbol{l}_m^{\boldsymbol{b}}(s) = \boldsymbol{l}_m^{\boldsymbol{b}}$, naturally defined from normalising the segment vector itself, cf. Figure 1(a). Then the alignment tensors per Burgers vector take the simple form,

$$\boldsymbol{\rho}^{(n),\boldsymbol{b}} = \frac{1}{|V|} \sum_{m=1}^{M(\boldsymbol{b})} L_{m,V}^{\boldsymbol{b}} \underbrace{\boldsymbol{l}_m^{\boldsymbol{b}} \otimes \cdots \otimes \boldsymbol{l}_m^{\boldsymbol{b}}}_{n\text{-times}}. \tag{15}$$

Note that $M(\boldsymbol{b})$ in this context denotes the number of segments with Burgers vector $\boldsymbol{b}$, not the number of dislocation loops.

All the alignment tensors are totally symmetric, i.e., any permutation π of the indices leaves the coefficients unchanged,

$$\rho_{i_{\pi(1)}\cdots i_{\pi(n)}}^{\boldsymbol{b}} = \rho_{i_1\cdots i_n}^{\boldsymbol{b}}. \tag{16}$$

Note that totally symmetric tensors of order n have far less independent components than general tensors of the same order. While a general tensor of order n in three dimensions has 3^n coefficients, totally symmetric tensors of order n only have $(n+2)(n+1)/2$ independent coefficients in 3D. Moreover, the definition above is reducible in the sense that the trace (i.e., the contraction of any two indices) of the nth order alignment tensor is the $(n-2)$th order alignment tensor [8],

$$\boldsymbol{\rho}^{(n-2),\boldsymbol{b}} = \mathrm{tr}\, \boldsymbol{\rho}^{(n),\boldsymbol{b}}. \tag{17}$$

The determination of the nth order tensor, given that the $(n-2)$th order tensor is known, consequently only requires the determination of $2n+1$ new coefficients. For example, the trace of the second order alignment tensor ($n=2$) is the total dislocation density, $\sum_i \rho^{\boldsymbol{b}}_{ii} = \rho^{\boldsymbol{b}}$. If the latter is known, it is enough to determine two of the diagonal elements and the three off-diagonal elements of the second order tensor. Alternatively, one may determine the two highest order alignment tensors of interest (with consecutive order), and with that all the lower order tensors can be evaluated using trace operations.

In the following section, we will discuss the information contained in the tensors of increasing order using several dislocation configurations obtained from DD simulations. However, prior to that we shall also introduce two additional tensor series which are related to line-curvature information. These tensors first appeared in evolution equations in CDD [8], but they were later realised as the carriers of interesting complementary information to the alignment tensors of their own right, in that they contain for instance topological information connected to the number of dislocation loops. The fact that we deal with curvature information, may let their definition appear difficult for descriptions based on straight segments. However, since the current definitions for volumes are based on integrals, the discrete determination of the curvature tensors is not much more complicated than for the alignment tensors. Once again, we begin with the definition for smooth curves.

The curvature vector $\boldsymbol{k}^{\boldsymbol{b}}_m(s)$ of a parametrised curve at $\boldsymbol{c}^{\boldsymbol{b}}_m(s)$ is defined as

$$\boldsymbol{k}^{\boldsymbol{b}}_m(s) = \frac{1}{\left|\partial_s \boldsymbol{c}^{\boldsymbol{b}}_m(s)\right|} \frac{\partial}{\partial s}\left(\boldsymbol{l}^{\boldsymbol{b}}_m(s)\right). \tag{18}$$

The curvature vector is always perpendicular to the line direction, $\boldsymbol{k}^{\boldsymbol{b}}_m(s) \perp \boldsymbol{l}^{\boldsymbol{b}}_m(s)$. The series of curvature tensors has by definition a vanishing scalar $q^{(0),\boldsymbol{b}} = 0$ and is defined for $n \geq 1$ as

$$\boldsymbol{q}^{(n),\boldsymbol{b}} = \frac{1}{|V|}\sum_{m=1}^{M(\boldsymbol{b})}\int_0^{S^{\boldsymbol{b}}_{m,V}} \mathrm{sym}\left(\boldsymbol{k}^{\boldsymbol{b}}_m(s) \otimes \underbrace{\boldsymbol{l}^{\boldsymbol{b}}_m(s) \otimes \cdots \otimes \boldsymbol{l}^{\boldsymbol{b}}_m(s)}_{(n-1)\text{-times}}\right)\left|\partial_s \boldsymbol{c}^{\boldsymbol{b}}_m(s)\right| \mathrm{d}s \tag{19}$$

$$= \frac{1}{|V|}\sum_{m=1}^{M(\boldsymbol{b})}\int_0^{S^{\boldsymbol{b}}_{m,V}} \frac{1}{n}\frac{\partial}{\partial s}\left(\underbrace{\boldsymbol{l}^{\boldsymbol{b}}_m(s) \otimes \cdots \otimes \boldsymbol{l}^{\boldsymbol{b}}_m(s)}_{n\text{-times}}\right)\mathrm{d}s \tag{20}$$

$$= \frac{1}{|V|}\frac{1}{n}\sum_{m=1}^{M(\boldsymbol{b})}\left(\underbrace{\boldsymbol{l}^{\boldsymbol{b}}_m(S^{\boldsymbol{b}}_{m,V}) \otimes \cdots \otimes \boldsymbol{l}^{\boldsymbol{b}}_m(S^{\boldsymbol{b}}_{m,V})}_{n\text{-times}} - \underbrace{\boldsymbol{l}^{\boldsymbol{b}}_m(0) \otimes \cdots \otimes \boldsymbol{l}^{\boldsymbol{b}}_m(0)}_{n\text{-times}}\right), \tag{21}$$

where sym denotes the operation of complete symmetrisation of a tensor. The curvature density tensor is consequently based on the overall change of direction of curves in V. Accordingly, closed curves in V, i.e., with $\boldsymbol{c}^{\boldsymbol{b}}_m(S^{\boldsymbol{b}}_{m,V}) = \boldsymbol{c}^{\boldsymbol{b}}_m(0)$ and $\boldsymbol{l}^{\boldsymbol{b}}_m(S^{\boldsymbol{b}}_{m,V}) = \boldsymbol{l}^{\boldsymbol{b}}_m(0)$ do not contribute to these tensors and non-trivial contributions only result from dislocations threading the volume; from the difference of the line tangents at the points of leaving and entering the volume. Without going into details we note that this shows that the average curvature tensors $\boldsymbol{q}^{(n),\boldsymbol{b}}$ equal a surface integral of alignment tensors, which is expressed in continuum variables by the relation $\boldsymbol{q}^{(n),\boldsymbol{b}} = 1/(n+1)\mathrm{div}\boldsymbol{\rho}^{(n+1),\boldsymbol{b}}$ [8].[2] Note that in order to recover the integral version of this in the

[2] In [8] there appears a different prefactor on the right hand side of this relation. This stems from a specific normalisation in the continuous case, which we don't employ in the current context.

discrete case would require obtaining the alignment tensors for oriented surface-patches instead of per volume as introduced in the current work.

The curvature tensors are well-defined and easily derived for straight segments as well. To this end, we need to think of integrals with a range of integration which includes the nodes where two dislocation segments meet and the line direction changes discontinuously. The result of such an integral still makes sense, where the curvature has to be considered as generalised function, i.e. a Schwartz distribution, at the kink[3] and the result will be based on the tangent directions of the adjacent segments. Since these tangents are constant away from the node, the exact start and end points of this integration do not matter and we assign the tensorial curvature contribution of two adjacent line segments to the shared node. By labelling the nodes as k and denoting the segment directions before and after the nodes (according to the common direction of integration) with $\boldsymbol{l}_k^{\boldsymbol{b}-}$ and $\boldsymbol{l}_k^{\boldsymbol{b}+}$, respectively (see Figure 1(b)), we attain the consistent definition of the volume based curvature tensors for distributions of straight segments as

$$\boldsymbol{q}^{(n),\boldsymbol{b}} = \frac{1}{|V|}\frac{1}{n}\sum_{k=1}^{K(\boldsymbol{b})}\left(\underbrace{\boldsymbol{l}_k^{\boldsymbol{b}+}\otimes\cdots\otimes\boldsymbol{l}_k^{\boldsymbol{b}+}}_{n\text{-times}} - \underbrace{\boldsymbol{l}_k^{\boldsymbol{b}-}\otimes\cdots\otimes\boldsymbol{l}_k^{\boldsymbol{b}-}}_{n\text{-times}}\right). \tag{22}$$

Note that we keep the classification by Burgers vector and $K(\boldsymbol{b})$ represents the number of nodes on dislocation lines with Burgers vector $\boldsymbol{b}$. The curvature density can also be defined for (multi-)junctions, if the junction is considered a segment for each involved elementary Burgers vector, such that the adjacent nodes are likewise assigned to several Burgers vectors simultaneously.

Though the above curvature tensors contain some information on global directional changes, they provide only surface information and are ignorant to interior changes of direction. This incompleteness is also apparent in the continuous case, where another series of curvature tensors is needed in addition for reconstructing a higher dimensional vectorial dislocation density [8]. The decisive quantity for these tensors is the "curvature weighted" binormal of the curve, which is defined as

$$\boldsymbol{k}_m^{*\boldsymbol{b}}(s) := \boldsymbol{l}_m^{\boldsymbol{b}}(s)\times\boldsymbol{k}_m^{\boldsymbol{b}}(s), \tag{23}$$

where $\times$ denotes the cross-product. We note that because $\boldsymbol{k}_m^{\boldsymbol{b}}(s)\perp\boldsymbol{l}_m^{\boldsymbol{b}}(s)$ holds $\left|\boldsymbol{k}_m^{*\boldsymbol{b}}(s)\right| = \left|\boldsymbol{k}_m^{\boldsymbol{b}}(s)\right| =: k_m^{\boldsymbol{b}}(s)$ and we find the commonly defined unit binormal of the curve as $\boldsymbol{b}_m^{\boldsymbol{b}}(s) = \boldsymbol{k}_m^{*\boldsymbol{b}}(s)/k_m^{\boldsymbol{b}}(s)$.

The auxiliary series of curvature tensors (again with a vanishing scalar $q^{*(0),\boldsymbol{b}}=0$) are defined for smooth curves and $n\geq 1$ as

$$\boldsymbol{q}^{*(n),\boldsymbol{b}} = \frac{1}{|V|}\sum_{m=1}^{M(\boldsymbol{b})}\int_0^{S_{m,V}^{\boldsymbol{b}}}\operatorname{sym}\left(\boldsymbol{k}_m^{*\boldsymbol{b}}(s)\otimes\underbrace{\boldsymbol{l}_m^{\boldsymbol{b}}(s)\otimes\cdots\otimes\boldsymbol{l}_m^{\boldsymbol{b}}(s)}_{(n-1)\text{-times}}\right)\left|\partial_s\boldsymbol{c}_m^{\boldsymbol{b}}(s)\right|\mathrm{d}s \tag{24}$$

$$= \frac{1}{|V|}\sum_{m=1}^{M(\boldsymbol{b})}\int_0^{S_{m,V}^{\boldsymbol{b}}}\operatorname{sym}\left(\left(\boldsymbol{l}_m^{\boldsymbol{b}}(s)\times\frac{\partial}{\partial s}\left(\boldsymbol{l}_m^{\boldsymbol{b}}(s)\right)\right)\otimes\underbrace{\boldsymbol{l}_m^{\boldsymbol{b}}(s)\otimes\cdots\otimes\boldsymbol{l}_m^{\boldsymbol{b}}(s)}_{(n-1)\text{-times}}\right)\mathrm{d}s \tag{25}$$

$$= \frac{1}{|V|}\sum_{m=1}^{M(\boldsymbol{b})}\int_0^{S_{m,V}^{\boldsymbol{b}}}\operatorname{sym}\left(\boldsymbol{l}_m^{\boldsymbol{b}}(s)\times\frac{\partial}{\partial s}\left(\underbrace{\boldsymbol{l}_m^{\boldsymbol{b}}(s)\otimes\cdots\otimes\boldsymbol{l}_m^{\boldsymbol{b}}(s)}_{n\text{-times}}\right)\right)\mathrm{d}s. \tag{26}$$

[3] Here, the term kink only refers to discontinuous changes in line direction in the numerical representation of a dislocation by straight segments and not to atomic kinks of the dislocations themselves.

Unlike for the curvature tensors, this integral may not be solved analytically such that it may not be as naturally defined for the straight segment case. Nevertheless, the curvature and consequently also the derivative of the tensor-products appearing in (26) are defined for kinks in a distributional sense. At nodes k with parameter s_k we have,

$$\frac{\partial}{\partial s}\left(\underbrace{\boldsymbol{l}_m^{\boldsymbol{b}}(s)\otimes\cdots\otimes\boldsymbol{l}_m^{\boldsymbol{b}}(s)}_{n\text{-times}}\right)=\left(\underbrace{\boldsymbol{l}_k^{\boldsymbol{b}+}\otimes\cdots\otimes\boldsymbol{l}_k^{\boldsymbol{b}+}}_{n\text{-times}}-\underbrace{\boldsymbol{l}_k^{\boldsymbol{b}-}\otimes\cdots\otimes\boldsymbol{l}_k^{\boldsymbol{b}-}}_{n\text{-times}}\right)\delta(s-s_k), \tag{27}$$

with a Dirac delta-distribution δ at s_k. However, if this is inserted into (26) this requires evaluating the line direction (occurring as factor in the cross-product) in the kink, where it is not uniquely defined. We suggest to define the tangent in the kink as the average tangent

$$\boldsymbol{l}_k^{\boldsymbol{b}}=\boldsymbol{l}^{\boldsymbol{b}}(s_k):=\frac{\boldsymbol{l}_k^{\boldsymbol{b}+}+\boldsymbol{l}_k^{\boldsymbol{b}-}}{\left|\boldsymbol{l}_k^{\boldsymbol{b}+}+\boldsymbol{l}_k^{\boldsymbol{b}-}\right|}. \tag{28}$$

In order to justify the choice of the average tangent we shall regard the first order auxiliary curvature vector, for which we obtain

$$\boldsymbol{q}^{*(1),\boldsymbol{b}}=\frac{1}{|V|}\sum_{k=1}^{K(\boldsymbol{b})}\boldsymbol{l}_k^{\boldsymbol{b}}\times\left(\boldsymbol{l}_k^{\boldsymbol{b}+}-\boldsymbol{l}_k^{\boldsymbol{b}-}\right). \tag{29}$$

We regard the difference of the two tangent vectors, i.e., the total change of direction, as the discrete curvature vector of the node, $\boldsymbol{k}_k^{\boldsymbol{b}}=\boldsymbol{l}_k^{\boldsymbol{b}+}-\boldsymbol{l}_k^{\boldsymbol{b}-}$. The curvature vector is perpendicular to the average line direction and the discrete auxiliary curvature vector $\boldsymbol{k}_k^{*\boldsymbol{b}}=\boldsymbol{l}_k^{\boldsymbol{b}}\times\boldsymbol{k}_k^{\boldsymbol{b}}$ is perpendicular to both, as is the case for their counterparts for smooth curves.

For defining the higher order auxiliary curvature tensors based on segments and in order to connect to the topological information contained in $\boldsymbol{q}^{*(1),\boldsymbol{b}}$, we provide an equivalent expression to (29), which follows from the antisymmetry of the cross product,

$$\boldsymbol{q}^{*(1),\boldsymbol{b}}=\frac{1}{|V|}\sum_{k=1}^{K(\boldsymbol{b})}\frac{1}{\left|\boldsymbol{l}_k^{\boldsymbol{b}+}+\boldsymbol{l}_k^{\boldsymbol{b}-}\right|}(\boldsymbol{l}_k^{\boldsymbol{b}-}\times\boldsymbol{l}_k^{\boldsymbol{b}+}-\boldsymbol{l}_k^{\boldsymbol{b}+}\times\boldsymbol{l}_k^{\boldsymbol{b}-}) \tag{30}$$

$$=\frac{1}{|V|}\sum_{k=1}^{K(\boldsymbol{b})}2\frac{\boldsymbol{l}_k^{\boldsymbol{b}-}\times\boldsymbol{l}_k^{\boldsymbol{b}+}}{\left|\boldsymbol{l}_k^{\boldsymbol{b}+}+\boldsymbol{l}_k^{\boldsymbol{b}-}\right|}. \tag{31}$$

We note that if $\boldsymbol{l}_k^{\boldsymbol{b}+}$ and $\boldsymbol{l}_k^{\boldsymbol{b}-}$ lie in a common plane with normal $\boldsymbol{n}_k$ we have

$$2\frac{\boldsymbol{l}_k^{\boldsymbol{b}-}\times\boldsymbol{l}_k^{\boldsymbol{b}+}}{\left|\boldsymbol{l}_k^{\boldsymbol{b}+}+\boldsymbol{l}_k^{\boldsymbol{b}-}\right|}=2\sin\left(\frac{\theta_k}{2}\right)\boldsymbol{n}_k, \tag{32}$$

where θ_k denotes the angle between the tangents, as depicted in Figure 1(b). Relation (32) may be shown by plane trigonometry and angle sum identities. Note that $2\sin(\theta_k/2)$ is a very good approximation for θ_k, deviating from the actual angle by less than 1% for angles smaller than 28° and less than 2% for angles below 39°. For a single closed planar curve in a plane with normal $\boldsymbol{n}$, when the curve is discretised by an increasing number of straight segments, the contribution of the curve to the auxiliary curvature vector hence quickly approximates the total angular change of a circulation, which is $2\pi\boldsymbol{n}$ according to Hopf's Umlaufsatz (e.g. [14]).

For the nth order tensor we generalise the definition in form (30) and obtain

$$\boldsymbol{q}^{*(n),\boldsymbol{b}}=\frac{1}{|V|}\sum_{k=1}^{K(\boldsymbol{b})}\frac{1}{\left|\boldsymbol{l}_k^{\boldsymbol{b}+}+\boldsymbol{l}_k^{\boldsymbol{b}-}\right|}\operatorname{sym}\left(\boldsymbol{l}_k^{\boldsymbol{b}-}\times\underbrace{\boldsymbol{l}_k^{\boldsymbol{b}+}\otimes\cdots\otimes\boldsymbol{l}_k^{\boldsymbol{b}+}}_{n\text{-times}}-\boldsymbol{l}_k^{\boldsymbol{b}+}\times\underbrace{\boldsymbol{l}_k^{\boldsymbol{b}-}\otimes\cdots\otimes\boldsymbol{l}_k^{\boldsymbol{b}-}}_{n\text{-times}}\right). \tag{33}$$

3. Analysis of dislocation distributions obtained from 3-dimensional DD

In this section we illustrate the information contained in the alignment and curvature tensors using the definitions provided above. For this purpose, we operate on discrete dislocation data obtained as direct output from ParaDis, an open source DD code [15]. This section consists of three analysis examples, where we start with a simple case and move on to analysing moderately complex dislocation distributions. At first, we consider the emission of dislocation loops from a Frank–Read source for validation of the concept, employing the natural interpretations of the alignment and curvature tensor quantities in this case. The rest of this section deals with the analysis of two dislocation configurations obtained by tensile loading from macroscopically similar initial configurations of randomly distributed glide loops. In this study, we limit the analysis up to second order alignment tensors and the first order curvature tensors, i.e., the determination of total dislocation density ρ, GND vector $\boldsymbol{\rho}^{(1)}$, second order alignment tensor $\boldsymbol{\rho}^{(2)}$, and the curvature vectors $\boldsymbol{q}^{(1)}$ and $\boldsymbol{q}^{*(1)}$. A summary of the employed definitions and of a few scalar measures introduced below is provided in Table A.3 of Appendix A.

We employ an in-house Matlab® code for calculating the alignment and curvature tensor quantities as well as for reconstruction and visualisation of dislocation line distributions. Nodal data files imported from ParaDis are used as input for the Matlab® script. This data file from ParaDis contains all information required for the reconstruction and subsequent evaluation of alignment and curvature tensors including domain size, nodal coordinates, neighbouring nodes, associated Burgers vector and plane normal. DD parameters for the Frank–Read source and the tensile test examples are listed in Table 1. These parameters are taken from the Frank–Read source and copper test cases of ParaDis V2.5.1.

3.1. *Validation and analysis of a simple dislocation configuration*

The dislocation configuration considered for validation is derived from a Frank–Read source[4] at a point in time, where it produced one closed dislocation loop and is about to emit a second one, as shown in Figure 2. The total dislocation density ρ is simply the sum over the length of all dislocation lines divided by the volume of the considered domain, and does not call for further analysis—though we checked that our evaluation coincides with the one provided by the ParaDis code. Also regarding the first order alignment tensor (the GND vector) $\boldsymbol{\rho}^{(1)}$ we have a very clear expectation. Since this is the vector sum of all line segments, we expect it to be the vector connecting the start and end point of the initial segment of the Frank–Read source (when multiplied with the volume of the considered domain). The results given in Table 2 show excellent agreement with this expectation.

The second order alignment tensor $\boldsymbol{\rho}^{(2)}$ is a symmetric positive semi-definite tensor, which shall be analysed by its eigenvalues and eigenvectors. The unit eigenvectors $\boldsymbol{e}_i$ form an orthonormal basis and indicate directions, $\boldsymbol{n}$, where the density of normally threading dislocations $\rho_{nn} = \boldsymbol{n} \cdot \boldsymbol{\rho}^{(2)} \cdot \boldsymbol{n}$ is extremal. The eigenvalues are the corresponding normal density in that direction, $\lambda_i = \rho_{e_i e_i}$. The eigenvalues will be ordered, such that $\lambda_1 \geq \lambda_2 \geq \lambda_3$. Since the considered Frank–Read source and its produced loop lie within a glide plane, the tensor represents a planar dislocation state. That is, one eigendirection is the slip plane normal with a vanishing eigenvalue. The other two eigenvalues are in the current case expected to be of similar magnitude, since the dislocation configuration has no strong orientation preference of the segments. This expectation is well met, cf. Table 2.

[4] For the current purpose it is immaterial that this source is manufactured from an unphysical open dislocation segment.

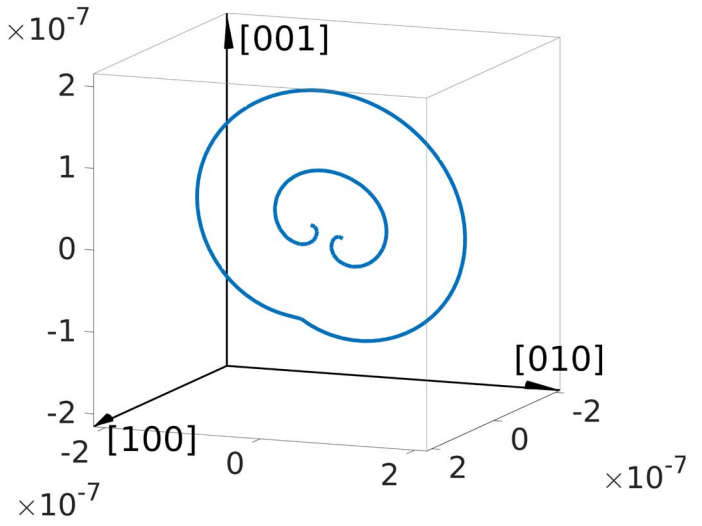

Figure 2. Dislocation configuration corresponding to a Frank–Read source simulated with ParaDis. The axis units are given in metre. The used parameters and conditions are provided in Table 1. The quantitative results of the analysis are given in Table 2.

Table 1. DD simulation parameters for Frank–Read source (Section 3.1) and multiple dislocation loops (Section 3.2)

Parameters/test conditions	Frank–Read source	Multiple dislocation loops	Unit
Simulation domain	$1000 \times 1000 \times 1000$	$1000 \times 1000 \times 1000$	$\lvert\boldsymbol{b}\rvert$
Mobility law	"FCC_0"	"FCC_0"	–
Burgers vector magnitude	2.875401×10^{-10}	2.55600×10^{-10}	m
Shear modulus	64.88424×10^{9}	54.6×10^{9}	Pa
Poisson's ratio	0.3327533	0.324	–
Fast Multipole Method (FMM)	Enabled	Enabled	–
FMM cellular Grid	$4 \times 4 \times 4$	$4 \times 4 \times 4$	–
Time step integrator	"Trapezoid"	"Trapezoid"	–
Minimum segment length	10.0	9.0	$\lvert\boldsymbol{b}\rvert$
Maximum segment length	50.0	20.0	$\lvert\boldsymbol{b}\rvert$
Edge dislocation mobility	1.0×10^{1}	1.0×10^{4}	$\mathrm{Pa}^{-1}{\cdot}\mathrm{s}^{-1}$
Screw dislocation mobility	1.0×10^{1}	1.0×10^{4}	$\mathrm{Pa}^{-1}{\cdot}\mathrm{s}^{-1}$
Load type	Creep	Constant strain rate	–
Maximum position error	1.0	1.0	$\lvert\boldsymbol{b}\rvert$
Strain rate	–	5.0×10^{6} in [0 0 1]-direction	s^{-1}
Applied stress	8.0×10^{9} in [0 0 1]-direction	–	Pa

The first order curvature tensor $\boldsymbol{q}^{(1)}$ can be obtained as the difference of the respective line directions at the end point and the start point of an open curve, or of a curve traversing a volume. Since the emitted loop is a closed curve, and the line directions of the start point and end point of the open line segment are in the regarded snapshot very similar, we expect the norm of the first

Table 2. Results of the analysis of the Frank–Read source. For the used simulation parameters, see Table 1

Physical quantity	Notation		Value	Unit
Volume of considered domain	V		8.024×10^{-20}	m^3
Total dislocation density	ρ		1.888×10^{13}	m^{-2}
Components of the	$\boldsymbol{\rho}^{(1)}$	$\rho^{(1)}_{[100]}$	-2.1502×10^{11}	m^{-2}
GND vector		$\rho^{(1)}_{[010]}$	4.3004×10^{11}	m^{-2}
		$\rho^{(1)}_{[001]}$	-2.1502×10^{11}	m^{-2}
Eigenvalues of the second	$\boldsymbol{\rho}^{(2)}$	λ_1	9.547×10^{12}	m^{-2}
order alignment tensor		λ_2	9.335×10^{12}	m^{-2}
		λ_3	9.657×10^{-4}	m^{-2}
Eigenvectors of the second	$\boldsymbol{\rho}^{(2)}$	$\boldsymbol{e}_1$	$(0.3950 \quad -0.8164 \quad 0.4213)^{\mathrm{T}}$	–
order alignment tensor		$\boldsymbol{e}_2$	$(-0.7146 \quad 0.0152 \quad 0.6994)^{\mathrm{T}}$	–
		$\boldsymbol{e}_3$	$(0.5774 \quad 0.5774 \quad 0.5774)^{\mathrm{T}}$	–
Degree of polarisation	$\pi = \dfrac{\lvert\boldsymbol{\rho}^{(1)}\rvert}{\rho}$		0.02789	–
Degree of alignment	$\alpha = \dfrac{\rho_{\mathrm{vM}}}{\rho}$		0.5001	–
First order curvature tensor	$\lvert\boldsymbol{q}^{(1)}\rvert$		1.139×10^{18}	m^{-3}
First order auxiliary curvature tensor	$\lvert\boldsymbol{q}^{*(1)}\rvert$		2.347×10^{20}	m^{-3}
Approximated number of circulations	$\nu = \dfrac{\lvert\boldsymbol{q}^{*(1)}\rvert\, V}{2\pi}$		2.997	–

order curvature tensor to be small compared to, for example, the norm of the first order auxiliary curvature tensor $\boldsymbol{q}^{*(1)}$. The results listed in Table 2 are also in line with this expectation.

As explained at the end of Section 2, for a planar curve, the first order auxiliary curvature tensor $\boldsymbol{q}^{*(1)}$ points in the direction of the slip plane normal and its norm is related to the number of circulations of the dislocation lines (if all have the same sense of circulation). For the Frank–Read source example, we expect three circulations in the considered state—exactly one for the closed emitted loop, and about two for the pinned dislocation line—one circulation from the start point to the midpoint and another from the midpoint to the endpoint. The norm of $\boldsymbol{q}^{*(1)}$ is therefore assumed to be close to three times 2π divided by the volume of the domain under consideration, which we find nicely confirmed in Table 1.

We close this section by introducing two measures for further analysis of the obtained quantities. A degree of polarisation $\pi = \lvert\boldsymbol{\rho}^{(1)}\rvert / \rho$ is defined as the ratio of the norm of the GND vector and the total dislocation density. The distribution of the Frank–Read source example with $\pi \approx 0.02789$, would be interpreted as weakly polarised. A degree of alignment, inspired by (but inverse to) the stress-triaxiality used to characterise stress states mostly in fracture and damage mechanics, can be defined in the present context. To this end, we employ a von Mises type equivalent density

$$\rho_{\mathrm{vM}} = \sqrt{\tfrac{1}{2}[(\lambda_1 - \lambda_2)^2 + (\lambda_2 - \lambda_3)^2 + (\lambda_1 - \lambda_3)^2]}. \tag{34}$$

The degree of alignment is then defined as

$$\alpha = \frac{\rho_{\mathrm{vM}}}{\rho}. \tag{35}$$

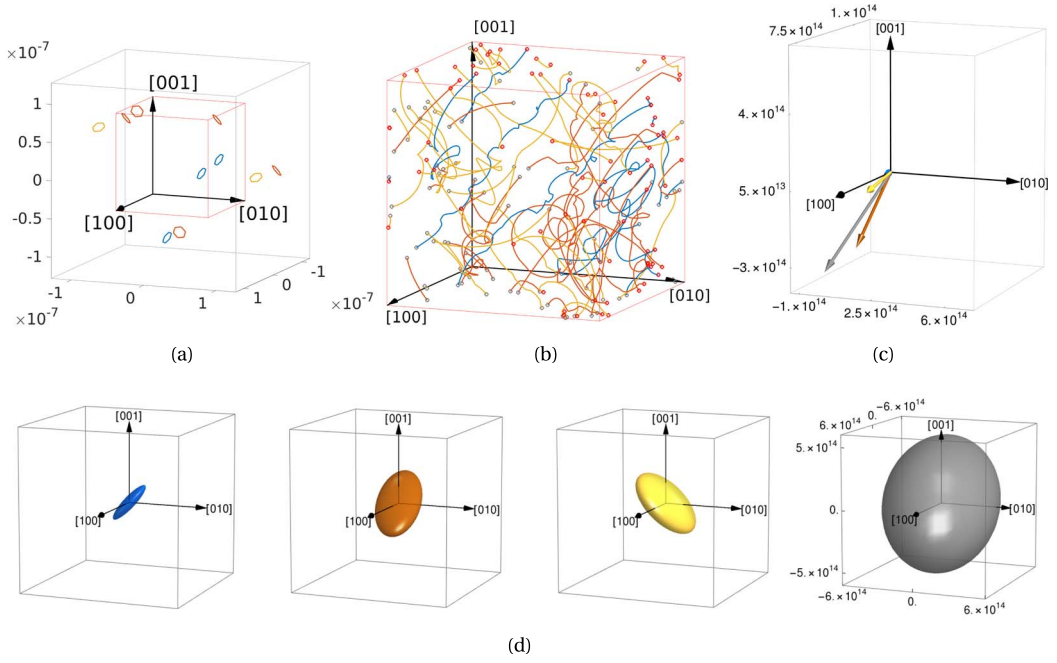

Figure 3. Example 1: (a) Initial condition of the DD simulation. Dislocation colouring according to Burgers vector: direction [011] in blue, $[1\,0\,\bar{1}]$ in orange, and $[0\,\bar{1}\,1]$ in yellow. Axis dimensions in metre. The sub-cube used for analysis is highlighted in red; (b) analysed dislocation distribution in the sub-cube after loading; (c) GND vectors $\boldsymbol{\rho}^{(1),\boldsymbol{b}}$ associated to Burgers vectors and the overall GND vector (grey). Axis dimensions in m^{-2}; (d) ellipsoids representing the second order alignment tensors (per Burgers vector and total). Axis dimensions in m^{-2}.

The degree of alignment is 1 for uniaxial alignment tensors ($\lambda_1 = \rho, \lambda_2 = \lambda_3 = 0$), takes the value 0.5 for biaxial alignment tensors ($\lambda_1 = \lambda_2 = \rho/2, \lambda_3 = 0$), and is 0 for triaxial alignment tensors ($\lambda_1 = \lambda_2 = \lambda_3 = \rho/3$). In the Frank–Read source example above, the degree of alignment nearly perfectly matches the biaxial value of 0.5, compare Table 2.

3.2. *Analysis of complex dislocation configurations*

In order to further illustrate the information contained in the alignment tensors, we evaluate them for two more complex dislocation distributions. In both cases, evaluation is performed for a sub-volume of the periodic simulation domain in order to have non-trivial dislocation density vectors $\boldsymbol{\rho}^{(1),\boldsymbol{b}}$, which would vanish if evaluated for the entire domain. This is also a good demonstration of how discretised fields may be obtained from DD simulations by subdividing the simulation box into sub-volumes; notably without the need to convert the discrete curves into continuous fields (D2C [9]) as intermediate step.

We present two examples, where the initial conditions of the periodic unit cells are indistinguishable in terms of the alignment and curvature tensors. The initial conditions are random distributions of the same number of equally sized hexagonal glide (all segments in the same slip system) loops with the same Burgers vectors as shown in Figures 3(a) and 4(a). The analysis of the tensors is restricted to a sub-cube of the unit cell with half the edge length of the full simulation domain, as indicated in the figures. A uniaxial extension with a constant strain rate is prescribed

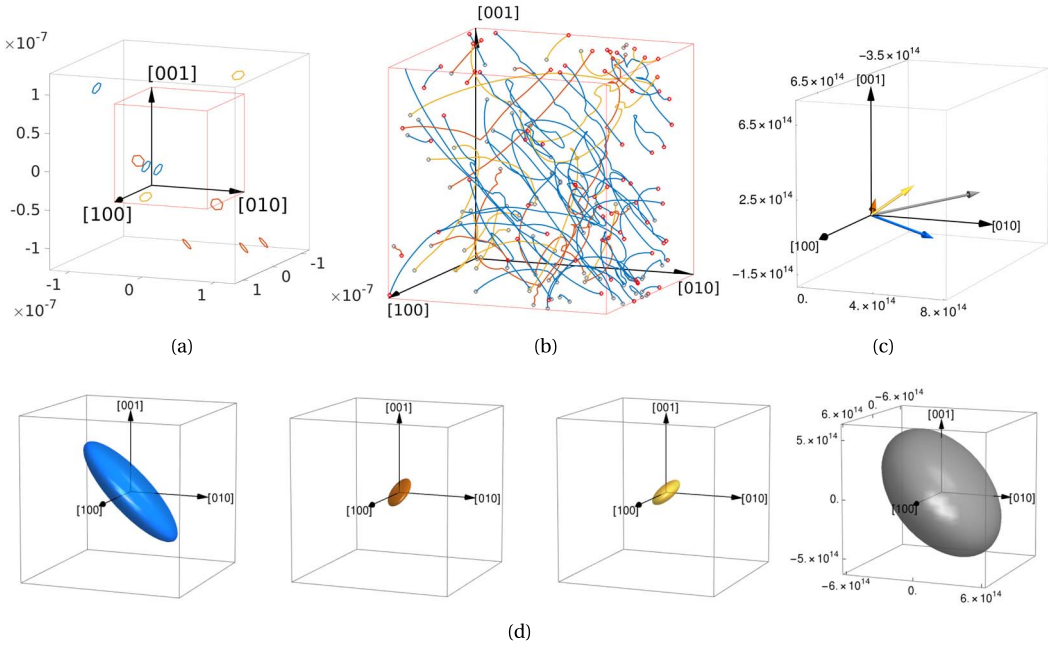

Figure 4. Example 2: (a) Initial condition of the DD simulation. Dislocation colouring according to Burgers vector: direction [011] in blue, $[1\,0\,\overline{1}]$ in orange, and $[0\,\overline{1}\,1]$ in yellow. Axis dimensions in metre. The sub-cube used for analysis is highlighted in red; (b) analysed dislocation distribution in the sub-cube after loading; (c) GND vectors $\boldsymbol{\rho}^{(1),\boldsymbol{b}}$ associated to Burgers vectors and the overall GND vector (grey). Axis dimensions in m^{-2}; (d) ellipsoids representing the second order alignment tensors (per Burgers vector and total). Axis dimensions in m^{-2}.

in the [001]-direction. The two regarded configurations are analysed at about the same strain, where a minor difference results from the variable time-stepping used in ParaDis.

The analysed configurations are displayed in Figures 3(b) and 4(b) respectively. In these figures, the dislocations are coloured according to Burgers vector. Intersection points of dislocations with the boundary of the evaluation domain are indicated red when they lie on the locally unique visible face of the cube and grey if they lie on the, likewise unique, rear face. In Figures 3(c) and 4(c), the obtained GND vectors classified by Burgers vector are displayed with arrows in the colours corresponding to the dislocations in the DD snapshots, while the overall GND vector is depicted in grey. The second order alignment tensors are displayed by ellipsoids, the axes of which are the eigenvectors, $\boldsymbol{e}_i$, scaled by corresponding eigenvalues λ_i, as provided in Tables A.1 and A.2 of Appendix A. The colouring scheme of the ellipsoids coincides with the one of the GND vectors. The overall volume of the ellipsoids exhibits the associated total dislocation density. The total dislocation density, degree of polarisation, and degree of alignment are additionally provided in Table 3.

Not surprisingly, the evolution of the two systems is quite distinct, at least on the level of the individual Burgers vectors. For symmetry reasons, the slip systems are of course equivalent and the physical significance of these differences is limited. However, in the current work, we do not seek to analyse the physical behaviour but rather focus on the potential of the alignment and curvature tensors for quantifying DD results in condensed form. As for the GND vectors $\boldsymbol{\rho}^{(1),\boldsymbol{b}}$, the evaluated degree of polarisation π of dislocations with given Burgers vector varies between

Table 3. Results of analysing the two DD simulations depicted in Figures 3(b) (Example 1) and 4(b) (Example 2)

Physical quantity	Notation	Example 1	Example 2	Unit
Volume of considered domain	V	2.087×10^{-21}	2.087×10^{-21}	m^3
Total dislocation density	ρ			m^{-2}
Burgers vector 1 (blue)		6.314×10^{14}	1.900×10^{15}	
Burgers vector 2 (orange)		1.112×10^{15}	5.181×10^{14}	
Burgers vector 3 (yellow)		1.231×10^{15}	6.195×10^{14}	
Total (grey)		2.975×10^{15}	3.038×10^{15}	
Degree of polarisation	$\pi = \dfrac{\lvert\boldsymbol{\rho}^{(1)}\rvert}{\rho}$			–
Burgers vector 1 (blue)		0.1498	0.2556	
Burgers vector 2 (orange)		0.3622	0.2239	
Burgers vector 3 (yellow)		0.3066	0.4720	
Total (grey)		0.2201	0.2384	
Degree of alignment, cf. (35)	$\alpha = \dfrac{\rho_{\mathrm{vM}}}{\rho}$			–
Burgers vector 1 (blue)		0.3904	0.3274	
Burgers vector 2 (orange)		0.3111	0.3164	
Burgers vector 3 (yellow)		0.2511	0.2336	
Total (grey)		0.1120	0.1400	

The DD simulation parameters are given in Table 1. We used different, but macroscopically indistinguishable initial conditions. The colours in the parentheses refer to Figures 3 and 4. The eigenvalues and eigendirections of the second order alignment tensors are provided in Tables A.1 and A.2 in Appendix A.

about 0.15 and 0.47 (Table 3). This suggests a relatively strong polarisation. However, more than anything else, this illustrates the well-known fact that the classification of dislocation densities into a geometrically necessary $\rho^{\boldsymbol{b}}_{\mathrm{GND}} = \lvert\boldsymbol{\rho}^{(1),\boldsymbol{b}}\rvert$ and a statistically stored fraction, $\rho^{\boldsymbol{b}}_{\mathrm{SSD}} = \rho^{\boldsymbol{b}} - \rho^{\boldsymbol{b}}_{\mathrm{GND}}$, is strongly scale dependent. Concerning the directions of the density vectors, we only state that they appear to be largely unrelated to the orientation of the ellipsoids obtained from the second order alignment tensors. Maybe the best illustration of the content of the second order alignment tensor is provided by the blue dislocations in Figure 4, which correspond to Burgers vector 1 in Example 2 in Table 3. The blue ellipsoid in Figure 4(d) clearly reflects the alignment of the blue dislocations in Figure 4(b) along the $\pm[0\,1\,\bar{1}]$-direction. The associated alignment tensor also shows a high degree of alignment with $\alpha = 0.3274$, which is only excelled by the value for the same Burgers vector in Example 1, which corresponds to the small blue ellipsoid in Figure 3(d). In Example 2, the strong alignment of the dislocations with the first Burgers vector also leads to a stronger overall alignment, as displayed by the grey ellipsoid in Figure 4(d) when compared to the one in Figure 3(d), as well as according to total degrees of alignment in Table 3. We finally note that none of the ellipsoids is pronouncedly oblate, which would indicate a planar distribution of dislocations, as given for each Burgers vector in the initial conditions. This may be attributed to the activation of cross-slip in the simulations, which enables dislocations to change their glide planes.

As for the curvature vectors, we concentrate on the auxiliary curvature vectors $\boldsymbol{q}^{*(1),\boldsymbol{b}}$, which are in the current cases larger than the curvature vectors $\boldsymbol{q}^{(1),\boldsymbol{b}}$ and more easily interpreted. We neglect the direction of the vectors and concentrate on their magnitude, which we analyse in

Table 4. Analysis and interpretation of quantities related to the auxiliary curvature vector $\boldsymbol{q}^{*(1)}$

Physical quantity	Notation	Example 1	Example 2	Unit
Net number of circulations	$\nu = \dfrac{\lvert\boldsymbol{q}^{*(1)}\rvert V}{2\pi}$			–
Burgers vector 1 (blue)		10.928	20.867	
Burgers vector 2 (orange)		14.544	4.371	
Burgers vector 3 (yellow)		10.612	5.296	
Net curvature	$\kappa = \dfrac{\lvert\boldsymbol{q}^{*(1)}\rvert}{\rho}$			m^{-1}
Burgers vector 1 (blue)		5.210×10^7	3.306×10^7	
Burgers vector 2 (orange)		3.936×10^7	2.540×10^7	
Burgers vector 3 (yellow)		2.594×10^7	2.574×10^7	

The colours in the parenthesis refer to Figures 3 and 4.

two ways: (*a*) though its relation to the number of circulations is only exactly given for planar loops, the ratio $\nu := \lvert\boldsymbol{q}^{*(1)}\rvert V/2\pi$ yields a lower bound for a kind of "number of circulations" for non-planar dislocations. We shall refer to ν as the net-number of circulations in the sequel. (*b*) Moreover, $\kappa := \lvert\boldsymbol{q}^{*(1)}\rvert/\rho$ may be interpreted (again with a grain of salt) as an average curvature. To see this, note that for a distribution of co-planar closed *circular* loops the inverse of κ, that is $\rho V/(\lvert\boldsymbol{q}^{*(1)}\rvert V)$ is the total line length divided by the number of loops times 2π, i.e. the average radius of the loops. We shall call κ the net-curvature in the sequel, because for 3D curves vectorial cancellations in the calculation of $\boldsymbol{q}^{*(1)}$ inhibit its direct interpretation as average curvature. The net number of circulations and the net curvature will only be analysed qualitatively, because the named interpretations solely apply strictly to planar loops. The results are provided in Table 4. In Example 1, the dislocations with Burgers vector 2 show a distinctly higher net number of circulations ν than the dislocations of Burgers vectors 1 and 3. This agrees with the visual impression that the orange dislocations are strongly entangled, especially in the lower right corner of Figure 3(b). Moreover, the blue dislocations (Burgers vector 1) have about the same ν-value like the yellow dislocations (Burgers vector 3), which yields a very high net curvature κ in case of the blue dislocations. Also this might be expected after a close inspection of the low right corner of the analysed region. In Example 2, the dominating blue dislocations also have by far the highest net number of circulations ν, but their net curvature κ is much lower than in Example 1. The latter also applies for Burgers vector 2, while there is nearly no difference between the examples for the κ-values of Burgers vector 3. Altogether, the lower net curvatures in Example 2 conform with the visual impression, that the dislocations in the second example appear less entangled than in the first one. The curvature information thus quantifies an aspect of the dislocation state which is likely to be of relevance for the further deformation of the system, both for the current "flow stress" as for dislocation multiplication and thus hardening.

4. Summary and conclusions

Large scale discrete dislocation simulations nowadays provide detailed insights in the plastic behaviour of crystals and the concomitant evolution of dislocation structures. However, regarding the evolving structures, the outcome of DD simulations are complex networks of lines or line segments which are notoriously difficult to analyse. In the current work, we presented a hierarchy of

tensorial dislocation density and curvature measures which characterise the geometry and partly topology of a dislocation network in a given volume with tunable degree of fidelity—where we anticipate that the number of tensor coefficients needed for a useful macroscopic characterisation will be very small as compared to the degrees of freedom (mostly determined by the number of segments) which define the dislocation distribution. The key results of the current paper are formulas (15), (22), and (33), which provide the recipe for calculating the tensorial measures from standard information provided in various DD codes, i.e., segments, nodes, and connectivity. We discussed the information contained in some of the lower order tensors with a simple example distribution obtained from a Frank–Read source which has emitted one loop and is in the course of creating a second one. Dislocation alignment tensors of up to second order and the auxiliary curvature vector were presented for two DD outcomes of tensile tests starting from macroscopically equivalent initial configurations. The depiction of the second order alignment tensors via ellipsoids illustrated how the tensor reflects apparent characteristics of the dislocation distributions. Dimensionless numbers were introduced to characterise the degree of polarisation and of alignment for dislocations of the same Burgers vector and for the dislocation network as a whole. The norm of the auxiliary curvature vectors were employed to define a net number of circulations and a net curvature which reflect qualitative impressions of entanglement of the dislocation configurations. For quick reference, a summary of important definitions is provided in Table A.3 of Appendix A.

We see an immense potential for employing the current tools in dislocation and plasticity research. To begin with, the tools are not limited to DD evaluations and may as well be applied to outcomes of molecular dynamic simulations or experimental measurements, once the dislocation information has been extracted. The tensors may thus be employed for comparing results obtained not only from different initial conditions but also with different methods. The tensors also lend themselves for being used in machine learning applications seeking to correlate macroscopic characteristics (e.g. flow stress or hardening, etc.) to characteristics of the underlying dislocation structure. Steinberger and co-authors [10] already demonstrated with machine learning techniques that the second order alignment tensor is of significance in distinguishing dislocation distributions. As for the curvature tensors we note for instance, that from the continuum theory we expect the vector $\boldsymbol{q}^{*(1)}$ to be intimately related to dislocation multiplication and thus hardening. Though the content of the higher order alignment and curvature tensors may be hard to conceive or to visualise, they provide highly condensed information on the dislocation state, which is likely to be exploitable by machine learning algorithms. In a spatially resolved form, based on multiple cells for which the tensorial measures would be evaluated, the current tools may provide discretised field quantities which can serve multiple purposes. On the one hand, a spatially refined analysis may be *per se* of interest, as it allows a more detailed analysis. On the other hand, the obtained results carry the potential of generating initial conditions or reference results for continuum based theories of dislocations, notably the continuum dislocation dynamics theories, which use these tensors as internal variables. Other future prospects would be to apply similar tensor expansions to evolving systems, for instance to dislocation fluxes in terms of segment velocities or swept surfaces (plastic shear). We also expect that the simple recipes for obtaining the tensors will facilitate the determination of spatial correlations in 3D dislocation configurations, notably for obtaining the correlation tensors already suggested by Kröner [16] and detailed by Zaiser in [17]. Last but not least, we believe that the dislocation density tensors may be the missing links for advancing the evaluation of X-ray diffraction patterns for other than just the GND information. Such a connection could be established from correlating the alignment tensors to virtual diffraction patterns [18–20] from DD results.

Appendix A.

Table A.1. Eigenvalues and eigenvectors of Example 1

Eigenvalue		Eigenvector			
Burgers vector 1 (blue)					
λ_1	3.646×10^{14}	$\boldsymbol{e}_1$	$(0.0562$	0.6934	$0.7183)^{\mathrm{T}}$
λ_2	1.829×10^{14}	$\boldsymbol{e}_2$	$(0.9722$	0.1258	$-0.1976)^{\mathrm{T}}$
λ_3	8.399×10^{13}	$\boldsymbol{e}_3$	$(-0.2274$	0.7094	$-0.6671)^{\mathrm{T}}$
Burgers vector 2 (orange)					
λ_1	5.767×10^{14}	$\boldsymbol{e}_1$	$(-0.6696$	-0.0761	$0.7388)^{\mathrm{T}}$
λ_2	3.578×10^{14}	$\boldsymbol{e}_2$	$(0.0096$	-0.9955	$0.0939)^{\mathrm{T}}$
λ_3	1.778×10^{14}	$\boldsymbol{e}_3$	$(0.7426$	-0.0558	$0.6674)^{\mathrm{T}}$
Burgers vector 3 (yellow)					
λ_1	5.762×10^{14}	$\boldsymbol{e}_1$	$(0.3947$	-0.6183	$0.6797)^{\mathrm{T}}$
λ_2	4.336×10^{14}	$\boldsymbol{e}_2$	$(0.9115$	0.1701	$-0.3745)^{\mathrm{T}}$
λ_3	2.215×10^{14}	$\boldsymbol{e}_3$	$(-0.1160$	-0.7674	$-0.6306)^{\mathrm{T}}$
Total (grey)					
λ_1	1.202×10^{15}	$\boldsymbol{e}_1$	$(-0.6456$	-0.0607	$0.7613)^{\mathrm{T}}$
λ_2	9.485×10^{14}	$\boldsymbol{e}_2$	$(0.2232$	-0.9683	$0.1121)^{\mathrm{T}}$
λ_3	8.245×10^{14}	$\boldsymbol{e}_3$	$(0.7304$	0.2423	$0.6387)^{\mathrm{T}}$

The colours in the parentheses refer to Figure 3.

Table A.2. Eigenvalues and eigenvectors of Example 2

Eigenvalue		Eigenvector			
Burgers vector 1 (blue)					
λ_1	1.007×10^{15}	$\boldsymbol{e}_1$	$(0.1209$	-0.6805	$0.7227)^{\mathrm{T}}$
λ_2	6.025×10^{14}	$\boldsymbol{e}_2$	$(0.9789$	0.2024	$0.0268)^{\mathrm{T}}$
λ_3	2.906×10^{14}	$\boldsymbol{e}_3$	$(-0.1645$	0.7042	$0.6907)^{\mathrm{T}}$
Burgers vector 2 (orange)					
λ_1	2.576×10^{14}	$\boldsymbol{e}_1$	$(-0.5570$	0.3291	$0.7626)^{\mathrm{T}}$
λ_2	1.898×10^{14}	$\boldsymbol{e}_2$	$(-0.5061$	-0.8624	$0.0025)^{\mathrm{T}}$
λ_3	7.069×10^{13}	$\boldsymbol{e}_3$	$(-0.6585$	0.3845	$-0.6469)^{\mathrm{T}}$
Burgers vector 3 (yellow)					
λ_1	2.736×10^{14}	$\boldsymbol{e}_1$	$(0.6953$	-0.4527	$-0.5582)^{\mathrm{T}}$
λ_2	2.329×10^{14}	$\boldsymbol{e}_2$	$(-0.6761$	-0.6755	$-0.2943)^{\mathrm{T}}$
λ_3	1.129×10^{14}	$\boldsymbol{e}_3$	$(0.2439$	-0.5820	$0.7757)^{\mathrm{T}}$
Total (grey)					
λ_1	1.266×10^{15}	$\boldsymbol{e}_1$	$(-0.1917$	-0.6878	$0.7002)^{\mathrm{T}}$
λ_2	9.958×10^{14}	$\boldsymbol{e}_2$	$(0.9789$	-0.1852	$0.0861)^{\mathrm{T}}$
λ_3	7.759×10^{14}	$\boldsymbol{e}_3$	$(0.0705$	0.7019	$0.7088)^{\mathrm{T}}$

The colours in the parentheses refer to Figure 4.

Table A.3. Summary of low order alignment tensors, curvature tensors and derived quantities

Symbol	Definition	Description
Alignment tensors		
$\rho^{\boldsymbol{b}}$	$\frac{1}{\lvert V\rvert}\sum_{m=1}^{M(\boldsymbol{b})} L^{\boldsymbol{b}}_{m,V}$	The *total dislocation density* counts the line length per volume.
$\boldsymbol{\rho}^{(1),\boldsymbol{b}}$	$\frac{1}{\lvert V\rvert}\sum_{m=1}^{M(\boldsymbol{b})} L^{\boldsymbol{b}}_{m,V}\boldsymbol{l}^{\boldsymbol{b}}_{m}$	The *vector of geometrically necessary dislocations (GND)* is equal to the vector sum of all line segments related to the volume.
$\boldsymbol{\rho}^{(2),\boldsymbol{b}}$	$\frac{1}{\lvert V\rvert}\sum_{m=1}^{M(\boldsymbol{b})} L^{\boldsymbol{b}}_{m,V}\boldsymbol{l}^{\boldsymbol{b}}_{m}\otimes\boldsymbol{l}^{\boldsymbol{b}}_{m}$	The *second order alignment tensor's* eigenvectors indicate directions where the density of normally threading dislocations is extremal. The eigenvalues are the corresponding normal density in that direction.
Curvature tensors		
$\boldsymbol{q}^{(1),\boldsymbol{b}}$	$\frac{1}{\lvert V\rvert}\sum_{k=1}^{K(\boldsymbol{b})}(\boldsymbol{l}^{\boldsymbol{b}+}_{k}-\boldsymbol{l}^{\boldsymbol{b}-}_{k})$	The *first order curvature vector* is the sum of all nodal curvature vectors per volume.
$\boldsymbol{q}^{*(1),\boldsymbol{b}}$	$\frac{1}{\lvert V\rvert}\sum_{k=1}^{K(\boldsymbol{b})}\boldsymbol{l}^{\boldsymbol{b}}_{k}\times(\boldsymbol{l}^{\boldsymbol{b}+}_{k}-\boldsymbol{l}^{\boldsymbol{b}-}_{k})$	For the calculation of the *first order auxiliary curvature vector*, the nodal curvature vectors are tilted by 90° by taking the cross product with the line direction, therefore pointing in the binormal direction, prior to summation.
Derived quantities		
π	$\frac{\lvert\boldsymbol{\rho}^{(1)}\rvert}{\rho}$	The *degree of polarisation* is defined as the ratio of the norm of the GND vector and the total dislocation density.
α	$\frac{\rho_{\mathrm{vM}}}{\rho}$	The *degree of alignment* is defined as the ratio of a von Mises type equivalent density (cf. (34)) to the total dislocation density. It is 1 for uniaxial alignment tensors, 0.5 for biaxial alignment tensors and 0 for triaxial alignment tensors.
ν	$\frac{\lvert\boldsymbol{q}^{*(1)}\rvert V}{2\pi}$	The *net number of circulations* gives an approximation to the number of dislocation circulations in the domain.
κ	$\frac{\lvert\boldsymbol{q}^{*(1)}\rvert}{\rho}$	The *net curvature* relates the norm of the auxiliary curvature vector to the total dislocation density, and is therefore independent of the domain size.

All terms are given per Burgers direction.

References

[1] M. D. Sangid, "Coupling in situ experiments and modeling — opportunities for data fusion, machine learning, and discovery of emergent behavior", *Curr. Opin. Solid State Mater. Sci.* **24** (2020), no. 1, article no. 100797.

[2] L. A. Zepeda-Ruiz, A. Stukowski, T. Oppelstrup, V. V. Bulatov, "Probing the limits of metal plasticity with molecular dynamics simulations", *Nature* **550** (2017), no. 7677, p. 492-495.

[3] S. I. Rao, C. Woodward, B. Akdim, E. Antillon, T. A. Parthasarathy, J. A. El-Awady, D. M. Dimiduk, "Large-scale dislocation dynamics simulations of strain hardening of ni microcrystals under tensile loading", *Acta Mater.* **164** (2019), p. 171-183.

[4] E. Kröner, "Allgemeine Kontinuumstheorie der Versetzungen und Eigenspannungen", *Arch. Ration. Mech. Anal.* **4** (1959), p. 273-334.

[5] E. Kröner, "Benefits and shortcomings of the continuous theory of dislocations", *Int. J. Solids Struct.* **38** (2001), no. 6–7, p. 1115-1134.

[6] G. Z. Voyiadjis, M. Yaghoobi, "Size and strain rate effects in metallic samples of confined volumes: Dislocation length distribution", *Scr. Mater.* **130** (2017), p. 182-186.

[7] R. B. Sills, N. Bertin, A. Aghaei, W. Cai, "Dislocation networks and the microstructural origin of strain hardening", *Phys. Rev. Lett.* **121** (2018), article no. 085501.

[8] T. Hochrainer, "Multipole expansion of continuum dislocations dynamics in terms of alignment tensors", *Philos. Mag.* **95** (2015), no. 12, p. 1321-1367.

[9] S. Sandfeld, G. Po, "Microstructural comparison of the kinematics of discrete and continuum dislocations models", *Model. Simul. Mater. Sci. Eng.* **23** (2015), no. 8, article no. 085003.

[10] D. Steinberger, H. Song, S. Sandfeld, "Machine learning-based classification of dislocation microstructures", *Front. Mater.* **6** (2019), p. 141-150.

[11] S. Hess, "Irreversible thermodynamics of nonequilibrium alignment phenomena in molecular liquids and in liquid crystals", *Z. Naturforsch.* **30a** (1975), p. 728-733.

[12] S. G. Advani, C. L. Tucker, "The use of tensors to describe and predict fiber orientation in short fiber composites", *J. Rheol.* **31** (1987), no. 8, p. 751-784.

[13] M. Kröger, "Flow-induced alignment of rod-like and flexible polymers in the molten state", *Physica A* **249** (1998), p. 332-336.

[14] A. N. Pressley, *Elementary Differential Geometry*, Springer-Verlag, 2001.

[15] M. Tang, G. Hommes, S. Aubry, A. Arsenlis, "ParaDIS-FEM dislocation dynamics simulation code primer", 2011, Technical Report, https://www.osti.gov/biblio/1037843/.

[16] E. Kröner, "Initial studies of a plasticity theory based upon statistical mechanics", in *Inelastic Behavior of Solids*, McGraw-Hill Book Company, New York, 1969, p. 137-147.

[17] M. Zaiser, "Local density approximation for the energy functional of three-dimensional dislocation systems", *Phys. Rev. B* **92** (2015), article no. 174120.

[18] L. Balogh, L. Capolungo, C. N. Tomé, "On the measure of dislocation densities from diffraction line profiles: A comparison with discrete dislocation methods", *Acta Mater.* **60** (2012), no. 4, p. 1467-1477.

[19] N. Bertin, W. Cai, "Computation of virtual X-ray diffraction patterns from discrete dislocation structures", *Comput. Mater. Sci.* **146** (2018), p. 268-277.

[20] D. Bamney, A. Tallman, L. Capolungo, D. E. Spearot, "Virtual diffraction analysis of dislocations and dislocation networks in discrete dislocation dynamics simulations", *Comput. Mater. Sci.* **174** (2020), article no. 109473.